Supplementary Information for 'Liquid-liquid Phase Transition in Supercooled H_2O and D_2O: A Path-Integral Computer Simulation Study'

Ali Eltareb[1,3], Gustavo E. Lopez[2,4], and Nicolas Giovambattista[1,3,4]

[1]*Department of Physics, Brooklyn College of the City University of New York, Brooklyn, New York 11210, United States*

[2]*Department of Chemistry, Lehman College of the City University of New York, Bronx, New York 10468, United States*

[3]*Ph.D. Program in Physics, The Graduate Center of the City University of New York, New York, NY 10016*

[4]*Ph.D. Program in Chemistry, The Graduate Center of the City University of New York, New York, NY 10016*

I. COMPUTER SIMULATIONS

We perform classical molecular dynamics (MD) and path-integral MD computer simulations (PIMD) of H_2O at the (T, P) indicated in Fig. S1. The state points studied using PIMD simulations of D_2O are also included. In all cases, the q-TIP4P/F water model [1] is employed.

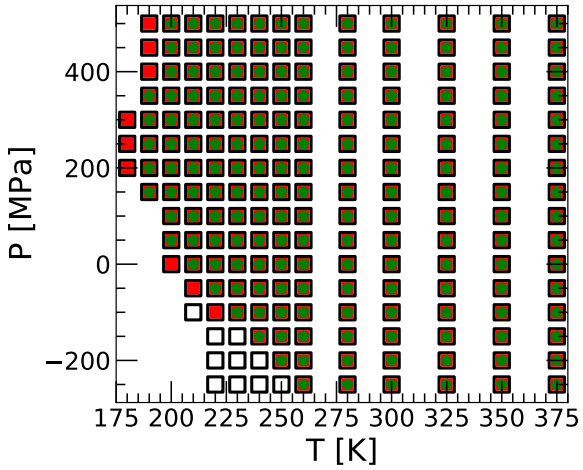

FIG. S1. State points studied in this work via classical MD and PIMD simulations of H_2O and D_2O using the q-TIP4P/F model. Black and red squares indicate, respectively, the state points studied using classical MD and PIMD simulations of H_2O. Green pentagons represent state points studied using PIMD simulations of D_2O.

II. ISOTHERMAL COMPRESSIBILITY AND ISOBARIC HEAT CAPACITY OF H_2O

Here, we address two points made in the main manuscript regarding H_2O. Specifically, (i) the isothermal compressibility of H_2O obtained from classical MD and PIMD simulations are identical, within error bars at most conditions studied; see Fig. S2. Again, this implies that nuclear quantum effects (NQE) (i.e., the delocalization of water atoms) play a minor role at approximately $T \geq 200$ K ($-100 \leq P \leq 400$ MPa), at least, in q-TIP4P/F water.

(ii) The isobaric heat capacity $C_P(T)$ is sensitive to the fitting procedure employed. In a

previous work [2], we calculate $C_P(T)$ by using the expression,

$$C_P(T) = \left(\frac{\partial H}{\partial T}\right)_{N,P} \tag{1}$$

where $H(T)$ was obtained by fitting the values for $H(T)$ obtained directly from the computer simulations using a fourth-order polynomial. As pointed out in the main manuscript, this procedure leads to a $C_P(T)$ that does not exhibit a maximum at low temperatures. As shown in Fig. S3(a), a fourth-order polynomial fits very well the values of $H(T)$ of H_2O obtained directly from our PIMD simulations. While the solid lines in Fig. S3(a) (fourth-order polynomial) and Fig. 4(a) of the main manuscript (TSEOS) both fit remarkably well the values of $H(T)$ from the PIMD simulations, the corresponding values of $C_P(T)$ obtained from Eq. 1 are qualitatively different. The C_P-maxima in Fig. 4(a) of the main manuscript are absent in the $C_P(T)$ of Fig. S3(b). Although $C_P(T)$ increases upon cooling at low pressures (Fig. S3(b)), as found in experiments, the rate at which $C_P(T)$ increases in our PIMD simulations is severely underestimated. At high pressures, experiments show that $C_P(T)$ decreases upon cooling, while our PIMD simulations show that $C_P(T)$ increases as the temperature decreases.

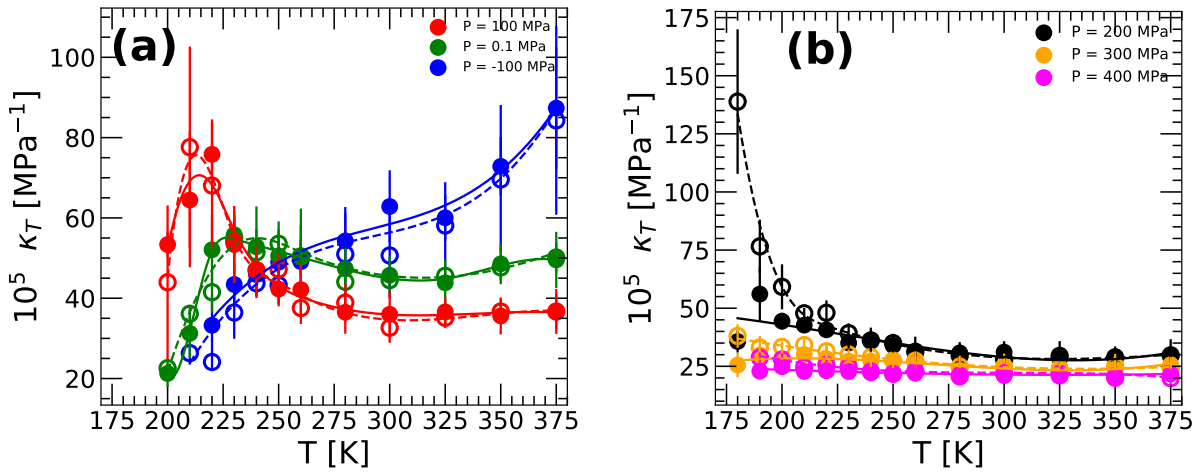

FIG. S2. Isothermal compressibility of H_2O from classical MD (empty circles) and PIMD simulations (solid circles; from Figs. 3(a) and 3(b) of the main manuscript) at selected pressures, above and below the LLCP pressure. The values of $\kappa_T(T)$ obtained from MD and PIMD simulations overlap within error bars. Lines are guides to the eye.

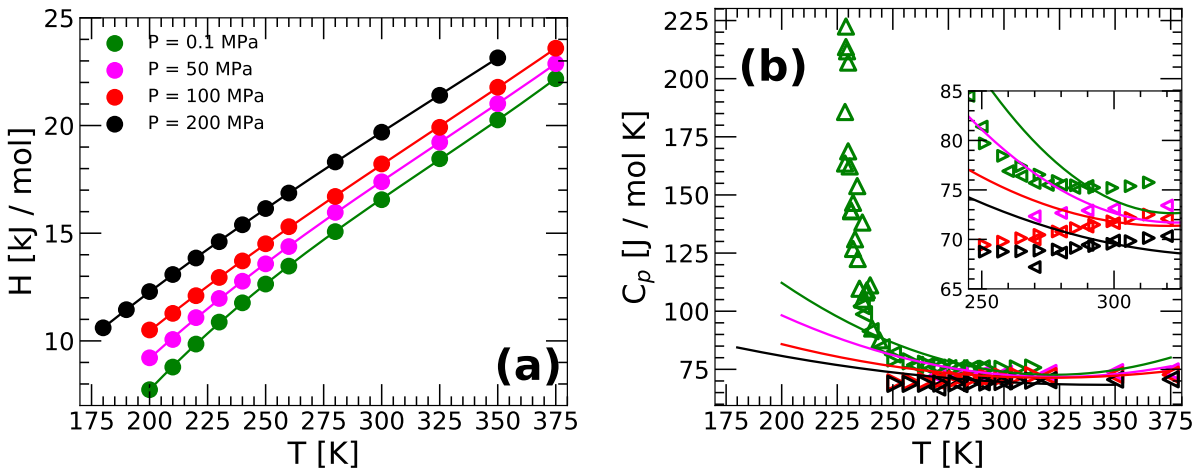

FIG. S3. (a) Enthalpy $H(T)$ of H_2O obtained from PIMD simulations at selected pressures (solid circles; from Fig. 4(a)). Lines are fits using a fourth-order polynomials. (b) Heat capacity $C_P(T)$ of H_2O obtained by differentiation of the fourth-order polynomials shown in (a). Results from PIMD simulations are indicated by solid lines; symbols are the corresponding experimental data (up-triangles are from Refs. [3]; left-triangles are from Refs. [4, 5]; right-triangles are from Refs. [6]). At low pressures, the fitting procedure employed here to calculate $H(T)$ leads to an increasing $C_P(T)$ upon cooling, in qualitative agreement with experiments, but there is no C_P-maximum at low temperatures, in disagreement with experiments. At high pressures, the behavior of $C_P(T)$ found in experiments and simulations is qualitatively different.

III. RESULTS FOR D_2O FROM PIMD SIMULATIONS

Next, we include results obtained from PIMD simulations of D_2O. Specifically, Fig. S4 shows the density of D_2O as function of temperature together with the corresponding TSEOS. The pressure and potential energy of the system along isotherms are included in Fig. S5. The $\kappa_T(T)$, $H(T)$, and $C_P(T)$ are shown, respectively, in Figs. S6, S7a, and S7b. The diffusion coefficient of D_2O is included in Fig. S8.

Overall, the results presented in Figs. S4-S8 for D_2O are qualitatively identical to those shown in Figs. 1-6 of the main manuscript for the case of H_2O. The main effect of isotope substitution H→D in water is mostly to shift the phase diagram of liquid water to higher temperatures by > 10 K; see Fig. S9.

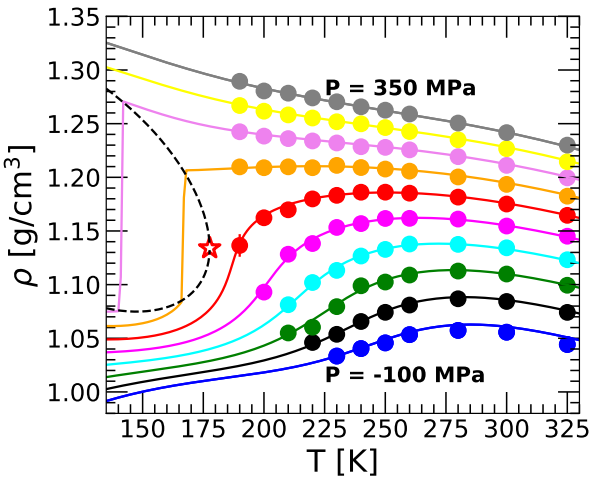

FIG. S4. Density of D_2O obtained from PIMD simulations using the q-TIP4P/F water model. Same as Fig. 1(d) of the main manuscript for the case of D_2O.

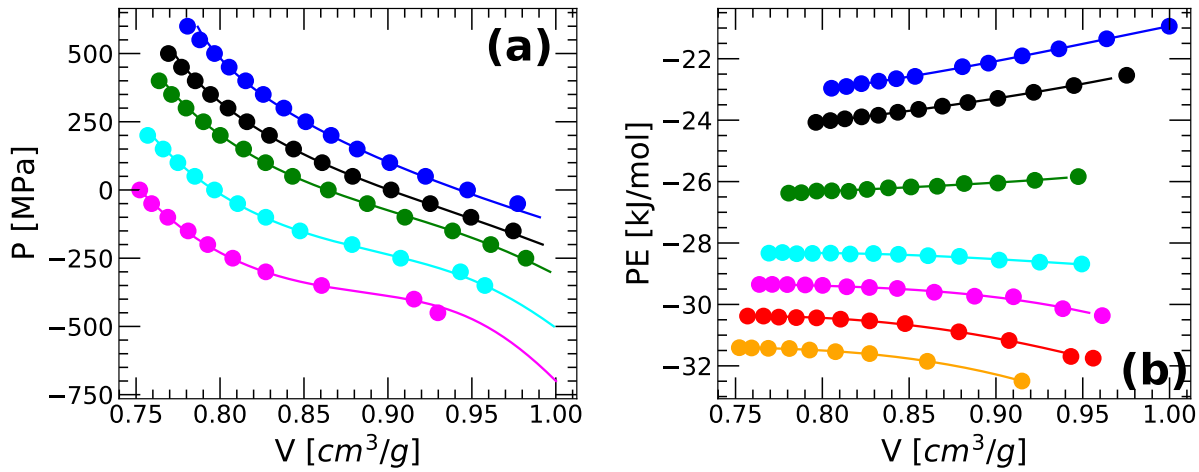

FIG. S5. (a) Pressure and (b) potential energy of D_2O as function of volume obtained from PIMD simulations of q-TIP4P/F water. Same as Figs. 2(b) and 2(c) of the main manuscript for the case of D_2O. In (a) isotherms correspond to (top to bottom) $T = 300,\ 260,\ 240,\ 220,\ 200$ K and are shifted by $\delta P = 100,\ 0,\ -100,\ -300,\ -500$ MPa, respectively. Temperatures in (b) are (top to bottom) $T = 375,\ 350,\ 300,\ 260,\ 240,\ 220,\ 200$ K.

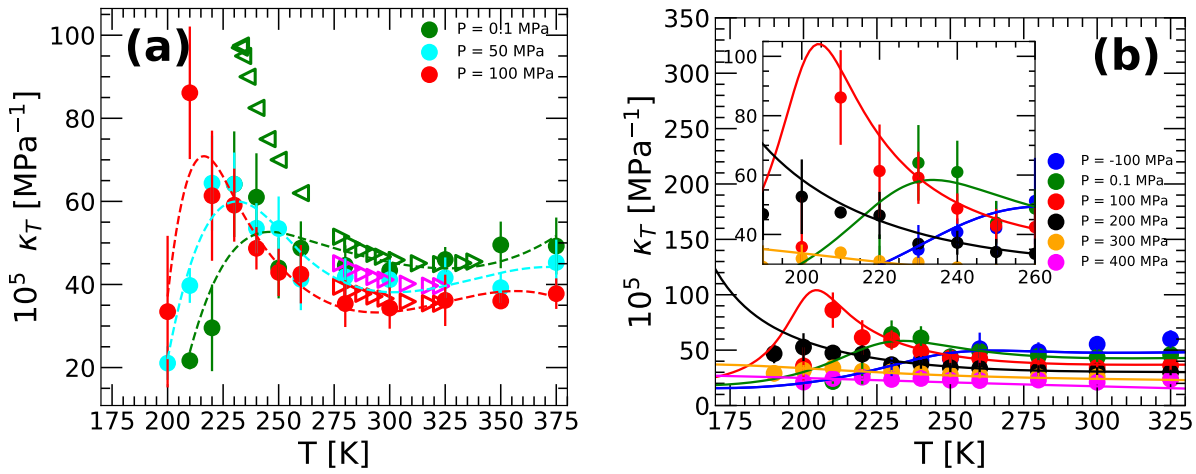

FIG. S6. Isothermal compressibility of D_2O from PIMD simulations using the q-TIP4P/F water model (compare with Fig. 3 of the main manuscript for H_2O). (a) Comparison between PIMD simulations (solid symbols) and experiments (empty symbols) [7–9]; dashed-lines are guide to the eye. (b) Comparison between PIMD simulations (solid symbols) and the corresponding predictions from the TSEOS (solid lines).

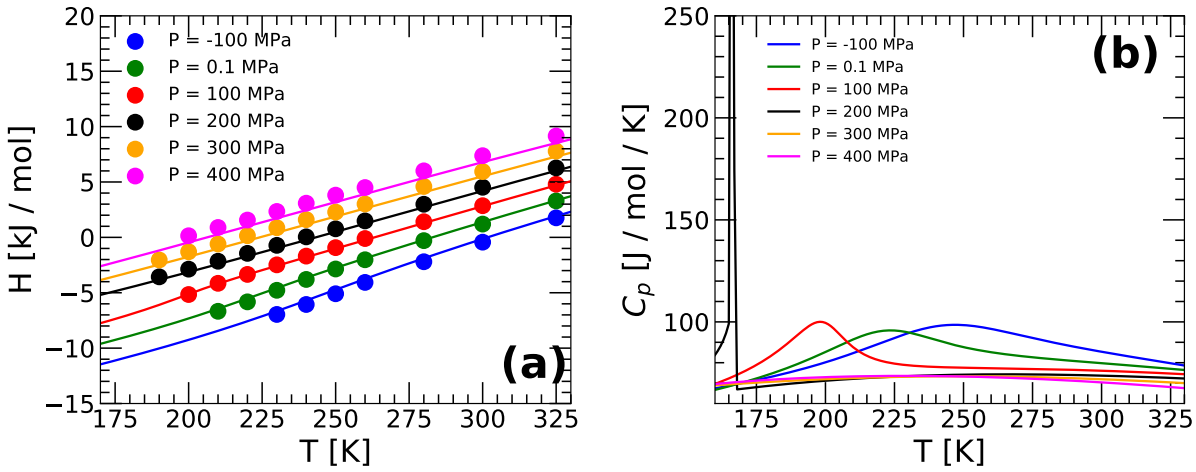

FIG. S7. (a) Enthalpy of D_2O from PIMD simulations using the q-TIP4P/F model (solid symbols). Lines are the predictions from the TSEOS. Same as in Fig. 4(a) of the main manuscript for the case of D_2O. (b) Isobaric heat capacity obtained from the TSEOS enthalpies shown in (a) by differentiation with respect to T. Same as Fig. 5(a) of the main manuscript for the case of D_2O.

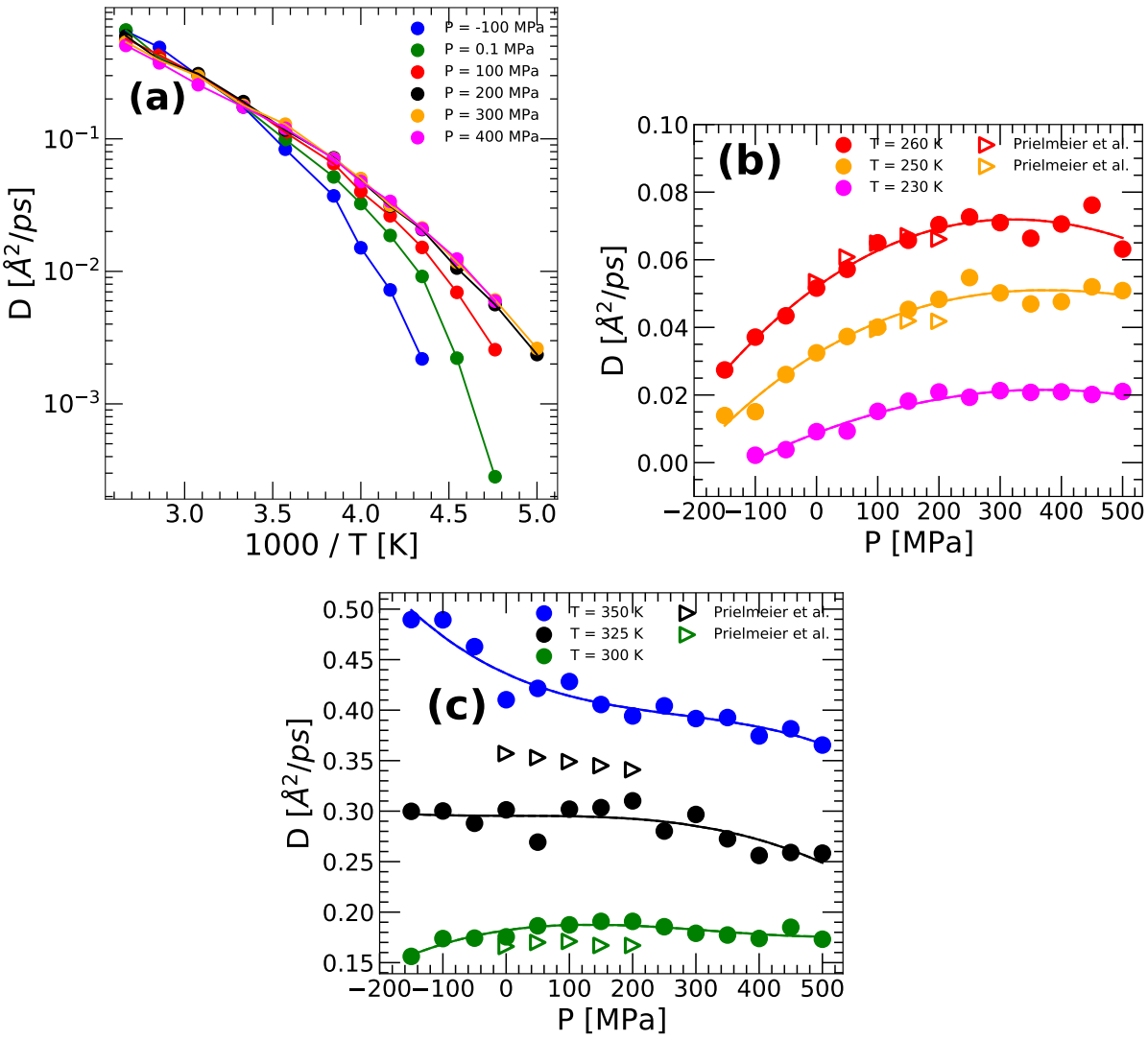

FIG. S8. (a) Diffusion coefficient of D_2O as a function of temperature from PIMD simulations using the q-TIP4P/F model. Same as Fig. 6(a) from the main manuscript for the case of D_2O. (b)(c) Diffusion coefficient of D_2O as a function of pressure; solid and empty symbols are results from PIMD simulations and experiments [10], respectively. Same as Figs. 6(b)-(c) from the main manuscript for the case of D_2O.

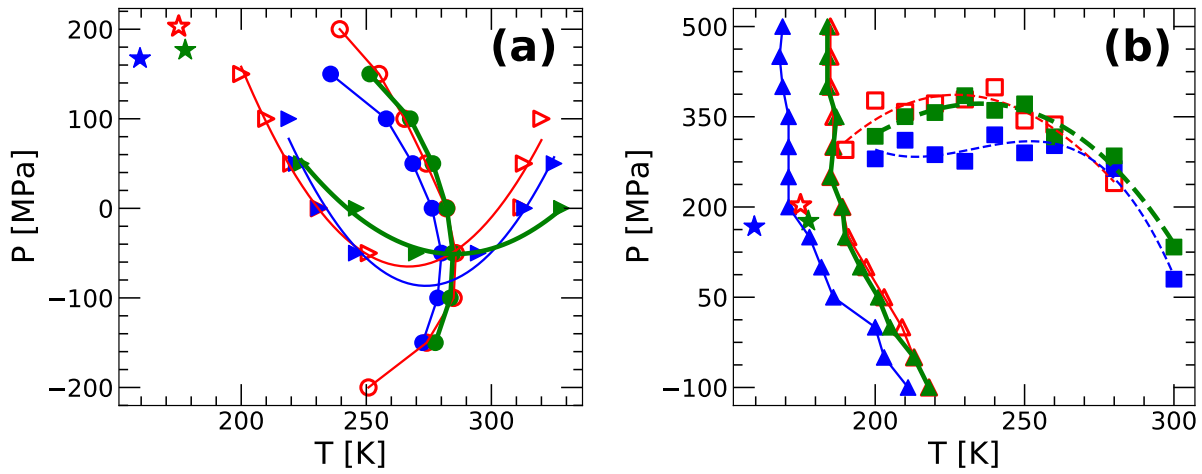

FIG. S9. NQE and isotope substitution effects on the phase diagram of q-TIP4P/F water. (a) Loci of ρ-maxima (circles), C_P-maxima (left triangles), and κ_T-maxima and minima (right-triangle); the stars represent the LLCP. Results for H_2O obtained from classical MD and PIMD simulations are shown with empty red and solid blue symbols, respectively; results for D_2O are shown by solid green symbols. (b) Locus of D-maxima (squares) and Mode Coupling temperature, $T_{MCT}(P)$ (up-triangles). NQE due to atoms delocalization tend to shift the phase diagram of water to lower T (red and blue symbols/lines). Similar effects follow due to isotope substitution ($D \rightarrow H$) (green and blue symbols/lines).

IV. TWO-STATE EQUATION OF STATE

The TSEOS provides an expression for the Gibbs free energy of the system, $G(N, P, T)$, in terms of 20 fitting parameters; details can be found in Refs. [11–13]. In this work, we follow the same procedure of Gartner *et al.* [11] paper. The software provided in Ref. [11] to obtain the TSEOS was used here with minor modifications to manipulate our data. The 20 parameters that fit our MD and PIMD simulation data are given in Tables S1-S3. Using these parameters, we calculate the $G(N, P, T)$ and hence, all thermodynamic properties, predicted by the TSEOS.

The pressures used to obtain the TSEOS are $-50 \leq P \leq 350$ MPa, which expand below and above the LLCP pressure. The temperatures used to obtain the TSEOS are $180 \leq T \leq 325$ K for H_2O and $190 \leq T \leq 325$ K for D_2O. The fitting parameters for the TSEOS based on the MD and PIMD simulation data are given in Table S1 and S2. Not surprisingly the values of T_c for H_2O and D_2O obtained in the main manuscript may shift slightly as additional temperatures closer to the LLCP are included to obtain the TSEOS.

To estimate the errors in (T_c, P_c, ρ_c), we used 50 different set of starting parameters and calculate the corresponding (T_c, P_c, ρ_c). Standard deviations in $(T_c,\ P_c,\ \rho_c)$ are included in Tables S1-S3. Briefly, we find that P_c can vary by about $10 - 25$ MPa, T_c varies by about $3 - 10$ K, and ρ_c can vary by about 0.01 g/cm^3.

	$180 \leq T \leq 325$ K (Classical)	$180 \leq T \leq 325$ K (Quantum)
ρ_c	1.03 (0.01)	1.02 (0.01)
P_c	203 (4)	167 (9)
T_c	175 (2)	159 (6)
λ	1.470	1.058
a	0.417	0.542
b	-0.299	-0.264
w_0	0.206	0.074
c_{00}	2.086	1.93
c_{01}	-0.008	-0.023
c_{02}	0.112	-0.027
c_{11}	-7.328	-4.922
c_{20}	-0.051	0.042
c_{12}	0.174	0.214
c_{21}	2.485	1.387
c_{30}	-0.031	-0.095
c_{22}	-0.036	-0.052
c_{31}	-0.449	-0.236
c_{40}	0.037	0.001
c_{23}	0.024	0.034
c_{32}	-0.026	0.005
c_{33}	-29.0	6.397

TABLE S1: LLCP coordinates and fitting parameters of the TSEOS for the case of H_2O from classical MD and PIMD simulations. Numbers in parenthesis are the standard deviations. T_c is in Kelvin, P_c is in MPa, and ρ_c is in g/cm^3.

	$190 \leq T \leq 325$ K
ρ_c	1.13 (0.01)
P_c	176 (2)
T_c	177 (3)
λ	1.084
a	0.430
b	-0.277
w_0	0.103
c_{00}	1.644
c_{01}	-0.020
c_{02}	-0.015
c_{11}	-4.416
c_{20}	0.031
c_{12}	0.219
c_{21}	0.947
c_{30}	-0.118
c_{22}	-0.044
c_{31}	-0.107
c_{40}	0.017
c_{23}	0.062
c_{32}	-0.009
c_{33}	-3.576

TABLE S2: Same as Table S1 for D_2O from PIMD simulations.

[1] S. Habershon, T. E. Markland, and D. E. Manolopoulos, J. Chem. Phys. **131**, 024501 (2009).

[2] A. Eltareb, G. E. Lopez, and N. Giovambattista, Phys. Chem. Chem. Phys. **23**, 6914 (2021).

[3] H. Pathak, A. Späh, K. Amann-Winkel, F. Perakis, K. K. H. Kim, and A. Nilsson, Mol. Phys. **117**, 3232 (2019).

[4] C. Angell, W. Sichina, and M. Oguni, J. Phys. Chem. **86**, 998 (1982).

[5] W. Wagner and A. Pruß, J. Phys. Chem. Ref. Data **31**, 387 (2002).

[6] J. Troncoso, J. Chem. Phys. **147**, 084501 (2017).

[7] K. H. Kim, A. Späh, H. Pathak, F. Perakis, D. Mariedahl, K. Amann-Winkel, J. A. Sellberg, J. H. Lee, S. Kim, J. Park, *et al.*, Science **358**, 1589 (2017).

[8] F. J. Millero and F. K. Lepple, J. Chem. Phys. **54**, 946 (1971).

[9] C.-T. A. Chen and F. J. Millero, J. Chem. Phys. **75**, 3553 (1981).

[10] F. Prielmeier, E. Lang, R. Speedy, and H.-D. Lüdemann, Berichte der Bunsengesellschaft für physikalische Chemie **92**, 1111 (1988).

[11] T. E. Gartner, L. Zhang, P. M. Piaggi, R. Car, A. Z. Panagiotopoulos, and P. G. Debenedetti, Proc. Natl. Acad. Sci. **117**, 26040 (2020).

[12] R. S. Singh, J. W. Biddle, P. G. Debenedetti, and M. A. Anisimov, J. Chem. Phys. **144**, 144504 (2016).

[13] J. W. Biddle, R. S. Singh, E. M. Sparano, F. Ricci, M. A. González, C. Valeriani, J. L. Abascal, P. G. Debenedetti, M. A. Anisimov, and F. Caupin, J. Chem. Phys **146**, 034502 (2017).